ASCE

# Half-Round Circular Crested Weir: On Hysteresis, Instabilities, and Head–Discharge Relationship

Hubert Chanson[1]

**Abstract:** Waters flowing over rounded weirs experience a rapidly accelerated flow region near the crest. The head-discharge relationship of a half-round crested weir was tested physically under carefully controlled flow conditions for a weir design with a small radius of curvature. The experiments were undertaken for a wide range of discharges, over two orders of magnitude, and the results were compared to the literature on circular weirs. The nappe was not aerated. With increasing discharges, the nappe was initially attached to the weir's downstream wall, until some nappe detachment occurred. With a further increase in flow rate, the detached nappe reattached at large flow rates. The transitions, i.e., both nappe detachment and reattachment, were characterized by large instabilities, change in flow properties, and sometimes loud noise, and the processes were subject to some hysteresis. The finding demonstrated the complicated features of an unaerated round-crested weir overflow. The importance of careful experimental procedure is discussed. **DOI: [10.1061/(ASCE)IR.1943-4774.0001473](10.1061/(ASCE)IR.1943-4774.0001473).** © 2020 American Society of Civil Engineers.

## Introduction

Weirs are hydraulic structures typically built across a river to facilitate the storage of water and raise the upstream water level (Novak et al. 2001). Small and large flows pass over the top of the weir wall. The crest of the weir is typically designed to maximize the discharge capacity, namely, to pass safely the design discharge at the lowest cost (Henderson 1966; USBR 1987). At the top of the crest, the specific energy is minimum and the flow conditions are called the critical flow conditions (Bakhmeteff 1912, 1932; Chanson 2006). The discharge characteristic curve of the structure is a function of the weir geometry, roughness, and inflow conditions (Miller 1994; Montes 1998; Chanson 2004). The unit flow rate $q$ is typically expressed as

$$q = \frac{Q}{B} = C_D \times \sqrt{g \times \left(\frac{2}{3} \times (H - P)\right)^3} \qquad (1)$$

where $Q$ = water discharge; $B$ = channel width; $C_D$ = dimensionless discharge coefficient; $g$ = gravity acceleration; $H$ = upstream total head; and $P$ = weir crest elevation above channel invert (Fig. 1). $C_D = 1$ for an ideal fluid overflow above a broad-crested weir. For $C_D > 1$, the discharge capacity is greater than that of a broad-crested weir for an identical upstream total head above crest $(H - P)$. The most common types of overflow linear weir are the broad-crested weir, the sharp-crested weir, the circular crested weir and the ogee-crest weir (Bos 1976; USBR 1987). The circular crested weir design is known for having a relatively large discharge capacity compared to broad-crested and sharp-crested weirs, its ease of passing floating debris, its simplicity of design, and lower cost.

[1]Professor in Hydraulic Engineering, School of Civil Engineering, Univ. of Queensland, Brisbane, QLD 4072, Australia. ORCID: https://orcid.org/0000-0002-2016-9650. Email: h.chanson@uq.edu.au

A recent test case study of round-crested weirs (Tullis et al. 2019) reported a number of discrepancies between 20 different hydraulic laboratory data sets across the world with the same specified geometry. The results presented "considerable scatter" in terms of the discharge coefficient. Tullis et al. (2019) listed a number of potential contributing parameters to the observed scatter and differences between laboratory results, without definite explanation. It is the aim of this study to provide a detailed characterization of the overflow above an unventilated half-round circular weir, including a discussion on the hysteresis and flow instabilities. The results contain some physical explanations for parts of the data scatter reported by Tullis et al. (2019).

## Nappe Overflow

In most applications, the approach flow is subcritical and the flow is critical at the weir crest. Owing to the streamline curvature, the pressure distribution is not hydrostatic and the velocity profile is not uniform at the crest (Fawer 1937; Vo 1992). A reanalysis of experimental observations showed that the solution of the critical flow depth followed closely (Chanson 2006, 2008):

$$\frac{d_{\text{crest}}}{H - P} \times \Lambda_{\text{crest}} = \frac{2}{3} \times \frac{1 - \cos(\delta/3) + \sqrt{3 \times (1 - [\cos(\delta/3)]^2)}}{2} \qquad (2)$$

where $d_{\text{crest}}$ = water depth at weir crest (Fig. 1); $\cos \delta = 1 - 2 \times \beta_{\text{crest}} \times C_D^2 \times \Lambda_{\text{crest}}^2$; $\Lambda$ = pressure correction coefficient; $\beta$ = momentum correction coefficient; $C_D$ = discharge coefficient; and subscript crest = flow properties at crest. For an ideal uniform flow above a flat broad crest with the streamlines parallel to the crest, the velocity distribution is uniform ($\beta = 1$), the pressure is hydrostatic ($\Lambda = 1$), and Eq. (2) yields the classical result

$$\frac{d_{\text{crest}}}{H - P} = \frac{2}{3} \qquad (3)$$

Downstream of the weir crest, the flow is accelerated by gravity. The flow depth $h$ and velocity $V$ derive from the equations of
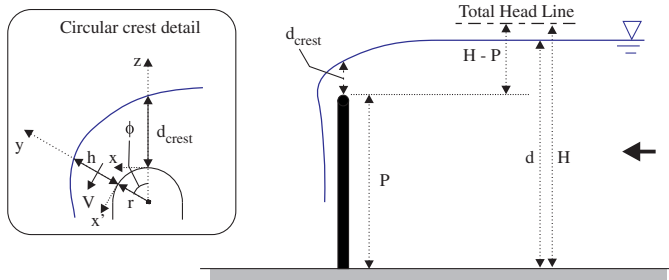
**Fig. 1.** Definition sketch of half-rounded circular weir overflow.

continuity and motion. For a one-dimensional ideal-fluid flow, this gives

$$\frac{h}{r} = \left(\frac{d_{\text{crest}}}{r}\right)^{3/2} \times C_D \times \sqrt{\frac{q^2}{g \times d_{\text{crest}}^3}} \times \frac{\sqrt{g \times r}}{V} \quad (4)$$

$$\frac{V}{\sqrt{g \times r}} = \sqrt{\left(\frac{V}{\sqrt{g \times r}}\right)^2 + 2 \times (1 - \cos\phi)} \quad (5)$$

with $r$ the radius of curvature (Fig. 1). At the surface of the circular weir invert, the invert pressure may be deduced from the motion equation in the radial direction. At an angular position $\phi > 0$, the dimensionless invert pressure equals

$$\frac{P_{\text{atm}} - P_{\text{wall}}}{\rho \times g \times r} = \frac{d}{r} \times \left(\left(\frac{V}{\sqrt{g \times r}}\right)^2 - \cos\phi \times \left(1 + \frac{d}{2 \times r}\right)\right) \quad (6)$$

where $P_{\text{wall}}$ = absolute invert pressure; $P_{\text{atm}}$ = atmospheric pressure; and $\rho$ = water density. In its gravitationless form, Eq. (6) was successfully compared with pressure distributions associated with the deflection of air jets blowing past circular quadrants (Fekete 1963; Sarpkaya 1968; Chanson 1998). The ideal-fluid flow calculation [Eq. (6)] predicts a suction pressure force acting on the flow along the downstream face of the weir, which increases with increasing velocity and increasing distance from the crest. When the absolute pressure of the fluid at the wall $P_{\text{wall}}$ falls below the vapor pressure $P_v$, the water next to the wall will vaporize and separation will occur through cavitation. In practice, cavitation

may take place at higher absolute pressures depending upon viscous, gravity and surface tension effects, the relative roughness, the water quality, and flow turbulence. Experimental observations suggested that, in a free-surface flow, cavitation occurs for

$$\frac{P_{\text{atm}} - P_v}{\frac{1}{2} \times \rho \times V^2} < \sigma_c \quad (7)$$

where $\sigma_c$ = critical cavitation number at which cavitation starts to appear, with $\sigma_c$ about 0.5–1 (e.g., Robertson 1965; Knapp et al. 1970).

## Experimental Facility, Instrumentation, and Methods

The investigation was conducted in the Hydraulics Laboratory of the Advanced Engineering Building (AEB) at the University of Queensland (UQ). Experiments were performed in a 3.0-m-long and 0.4-m-wide ($B = 0.40$ m) tilting flume. The bed and sidewalls of the flume were made of PVC and glass, respectively (Fig. 2). The bed of the channel was horizontal, i.e., $S_0 = \sin\theta = 0$, for all experiments to reduce the number of independent variables. Upstream of the flume, the water was supplied by a 0.75-m-long × 0.90-m-wide × 1.0-m-deep intake structure, fed by a constant head tank, and equipped with baffles, followed by a 0.54-m-long three-dimensional (3D) convergent leading to the 3.0-m-long × 0.4-m-wide flume. The intake structure and 3D convergent design allowed smooth inflow conditions at the flume's upstream end. At the downstream end, the flume ended with a free overfall.

A half-round circular crested weir was installed at 1.34 m downstream of the flume's upstream end, at a right angle across the flume. The weir was 0.020 m thick, with the crest height 250 mm above the invert ($P = 0.250$ m), based upon the design proposed by Tullis et al. (2019). The half-round crest had a 10.0-mm radius ($r = 0.010$ m) round over the upstream and downstream crest edges. Both the weir and crest were made of PVC, machined with an accuracy of ±0.2 mm.

The water discharge was measured using a volume-per-time technique and a 90° V-notch weir. The former was used for flow rates up to 0.015 m³/s, while the latter could be used with flow rates up to 0.120 m³/s (Chanson and Wang 2013). The percentage of error of the flow rate was less than 2%. A rail-mounted pointer gauge was used to measure the upstream free-surface elevation
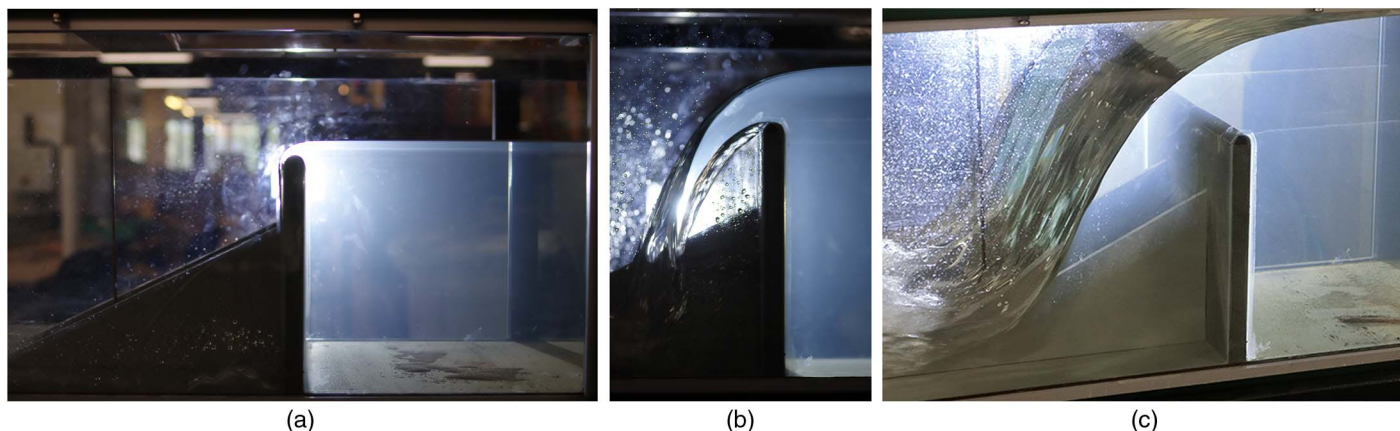


**Fig. 2.** Overflow experiments on half-round circular weir; flow direction from right to left: (a) attached nappe for $Q = 0.0016$ m³/s ($q = 0.004$ m²/s), $(d - P)/P = 0.060$—experiment with increasing flow rate; and (b) detached nappe for $Q = 0.0128$ m³/s ($q = 0.032$ m²/s), $(d - P)/P = 0.234$—experiment with increasing flow rate; and (c) attached nappe for $Q = 0.0378$ m³/s ($q = 0.0945$ m²/s), $(d - P)/P = 0.476$—experiment with decreasing flow rate.

© ASCE          04020008-2          J. Irrig. Drain. Eng.

J. Irrig. Drain Eng., 2020, 146(6): 04020008

**Table 1.** Flow conditions for different flow regimes above a half-round circular weir (current study)

| Experiments | Regime I | Regime II | Regime III |
|---|---|---|---|
| Increasing discharges | $(d - P)/P < 0.25$ | $0.25 < (d - P)/P < 0.34$ | $(d - P)/P > 0.34$ |
| | $(d - P)/r < 6.25$ | $6.25 < (d - P)/r < 8.5$ | $(d - P)/r > 8.5$ |
| Decreasing discharges | $(d - P)/P < 0.08 - 0.1$ | $0.08 - 0.1 < (d - P)/P < 0.3$ | $(d - P)/P > 0.3$ |
| | $(d - P)/r < 2 - 2.5$ | $2 - 2.5 < (d - P)/r < 7.5$ | $(d - P)/r > 7.5$ |



(a)  (b)  (c)
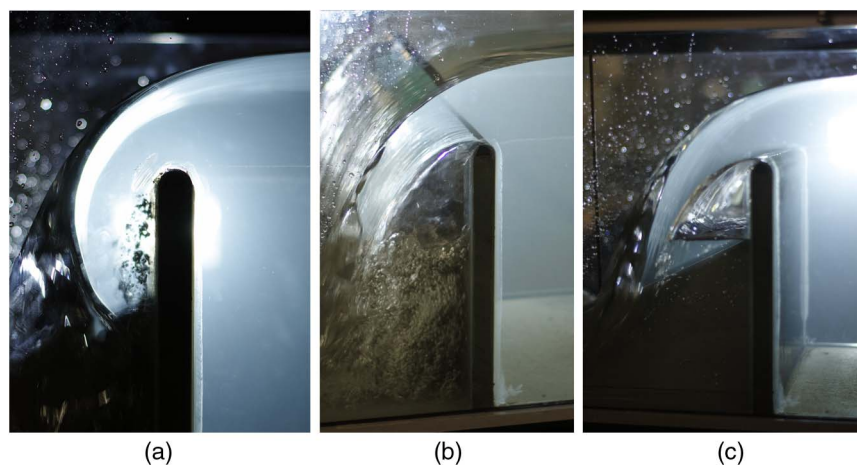
**Fig. 3.** Sequence of nappe detachment during a series of experiments with decreasing discharge. Flow conditions: $Q = 0.0217$ m³/s ($q = 0.05425$ m²/s), $(d - P)/P = 0.312$ (a) to 0.34 (b and c); flow direction from right to left: (a) attached nappe shortly before detachment at $t = t_0$ and $(H - P)/r = 8.73$—note formation of air pockets in undetached nappe; (b) detached nappe shortly after nappe detachment at $t = t_0 + 16$ s and $(H - P)/r = 7.64$—note very turbulent aerated flow beneath air cavity next to weir toe; and (c) detached nappe 1 min after nappe detachment at $t = t_0 + 61$ s and $(H - P)/r = 7.64$.

0.5 m upstream of the weir with an accuracy of ±0.5 mm and zeroed in situ. The depth above the weir crest was recorded through the glass sidewall. Photographic information on the experimental facility and flow patterns were further recorded using Pentax K-7 and Pentax K-3 digital single-lens reflex cameras, as well as with a Casio EX-10 Exilim digital camera with high-speed movie capability (Supplementary Data).

Experiments were performed for discharges between $3 \times 10^{-4}$ and $3.94 \times 10^{-2}$ m³/s, corresponding to unit discharges from $7.5 \times 10^{-4}$ to $9.85 \times 10^{-2}$ m²/s. For all experiments, the tailwater conditions were controlled only by the free overfall at the downstream end of the flume, and the nappe was unventilated. Following initial tests, some hysteresis was observed. Detailed experiments were repeated with both increasing and decreasing discharges. While the experimental readings were initially taken every 3 min, the nappe detachment and reattachment could occur over a longer period. Measurements for these flow conditions were undertaken after 30 min of stable flow conditions. Further steady-state experiments were undertaken for more than 1 h in a few cases to document some cyclic flow instabilities.

## Flow Patterns

Although the weir overflow was unventilated, three basic flow patterns were observed for different ranges of discharge (Fig. 2 and Table 1). At low flow rates, the overflow was undetached and the nappe remained attached to the downstream face of the weir wall (Regime I) [Figs. 1 and 2(a)]. For a range of intermediate discharges, the overflow became detached and a well-defined air cavity formed underneath the lower nappe, with a pool of water

forming at the toe of the weir wall (Regime II) [Fig. 2(b)]. The pool of water at the downstream toe of the weir was important because its weight provided the pressure force parallel to the channel invert required to change the momentum flow direction upon nappe impact (Moore 1943; Chanson 1995). At large discharges, the air cavity disappeared and the overflow reattached and was unaerated (Regime III) [Fig. 2(c)].

The current experimental observations showed, however, some hysteresis in the transitions between regimes. The flow conditions
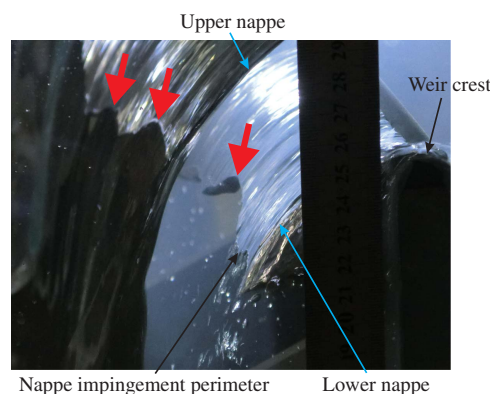


**Fig. 4.** Nappe instability for $Q = 0.0217$ m³/s ($q = 0.0543$ m²/s, $(d - P)/P = 0.344$, see Movie S2) during long-duration (1 h) steady-flow experiment—large transverse nappe instabilities are highlighted with thick arrows; Movie S2 presents further details of temporal instabilities of nappe.
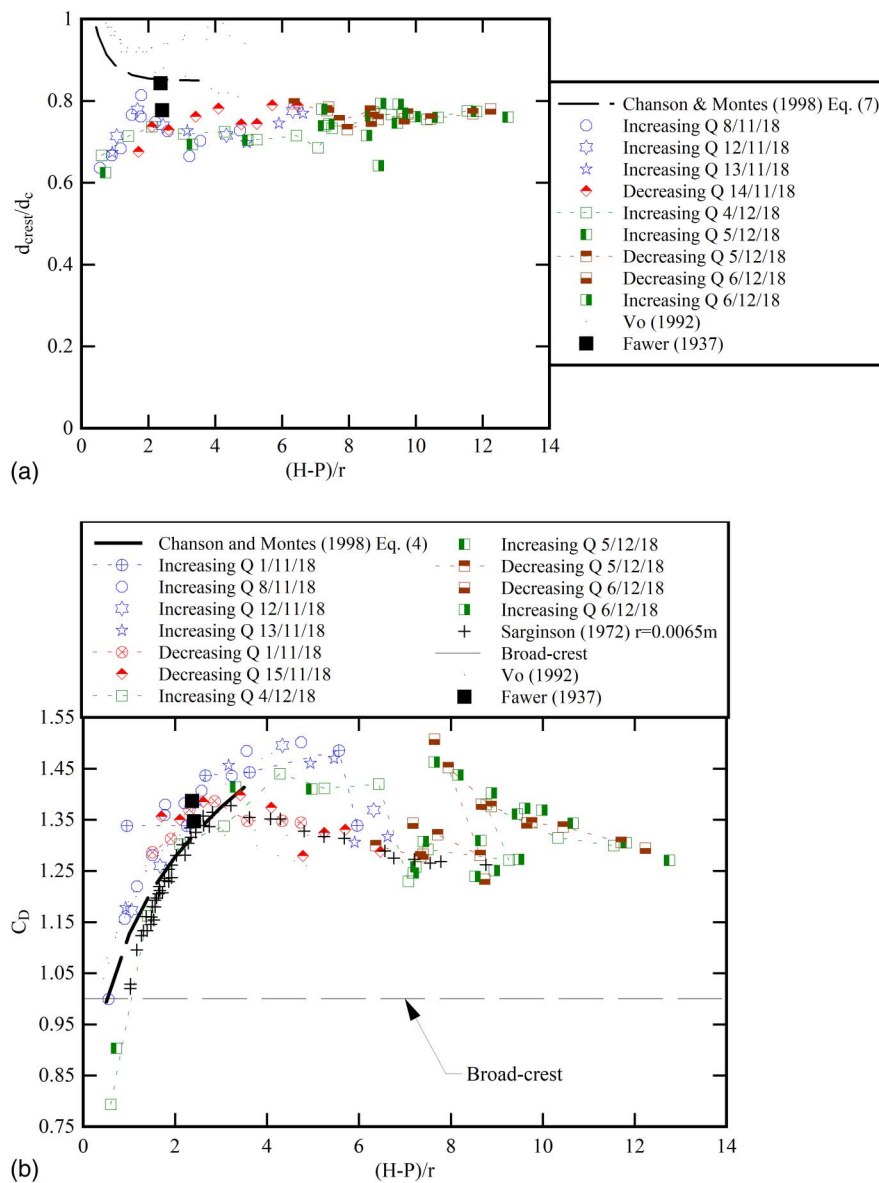
**Fig. 5.** Dimensionless water depth $d_{crest}/d_c$ at crest and discharge coefficient $C_D$ over half-round circular crest weir: (a) dimensionless water depth $d_{crest}/d_c$ at crest—comparison with data of Fawer (1937), Vo (1992), and Chanson and Montes (1998) (thick dashed line) on circular weirs; and (b) dimensionless discharge coefficient $C_D$—comparison between present data and data of Fawer (1937), Vo (1992), Sarginson (1972), and Chanson and Montes (1998) on circular weirs.

for the transition from Regime I to Regime II and from Regime II to Regime III were substantially different, whether the experiments were performed with increasing or decreasing discharges (Table 1). The present findings are summarized in Table 1. Herein $P$ and $r$ were kept constant following Tullis et al. (2019), and in Table 1, the variations in $(d - P)/P$ only represent the variation of upstream water depth $d$. This might affect any generalization of the results.

Physically, such a hysteresis was linked to the nonlinearities in the nappe detachment and reattachment processes, hydrodynamic instabilities, large pressure fluctuations, and weir vibrations (Ogihara and Maramatsu 1985; Wu and Plaut 1996; Chanson 1997). With increasing discharges, Regime I with an attached nappe was observed for small to medium flow rates, i.e., $(d - P)/P < 0.25$. Some air bubbles were observed in the undetached nappe for $(d - P)/P > 0.2$. Regime II occurred with a detached nappe for medium flow rates corresponding to $0.25 < (d - P)/P < 0.34$. Regime III with an undetached nappe was observed for large flow

rates corresponding to $(d - P)/P > 0.34$. In contrast, experiments with decreasing discharges showed different regime transition conditions (Fig. 3). Starting from a large flow rate, Regime III (undetached nappe) occurred for $(d - P)/P > 0.3$. A detached flow (Regime II) took place for $0.08 – 0.1 < (d - P)/P < 0.3$. Regime I with a reattached nappe was recorded for $(d - P)/P < 0.08$. However, a detached nappe with a very unstable cavity was seen for $0.08 < (d - P)/P < 0.14$. For one flow rate ($q = 0.05425$ m$^2$/s, $(d - P)/P \sim 0.3$), cyclic behavior was observed with the formation of a large air cavity, sometimes in an explosive manner with a loud noise, followed by the slow filling of the air cavity (12- to 15-min period), then the air cavity closure/disappearance, and again a very sudden cavity reopening into a large air cavity.

Further long-duration experiments were conducted for steady flow rates with $0.285 < (d - P)/P < 0.35$, with a minimum duration of 30 min up to more than 1 h. These observations showed cyclic behavior with cavity filling followed by attached nappe
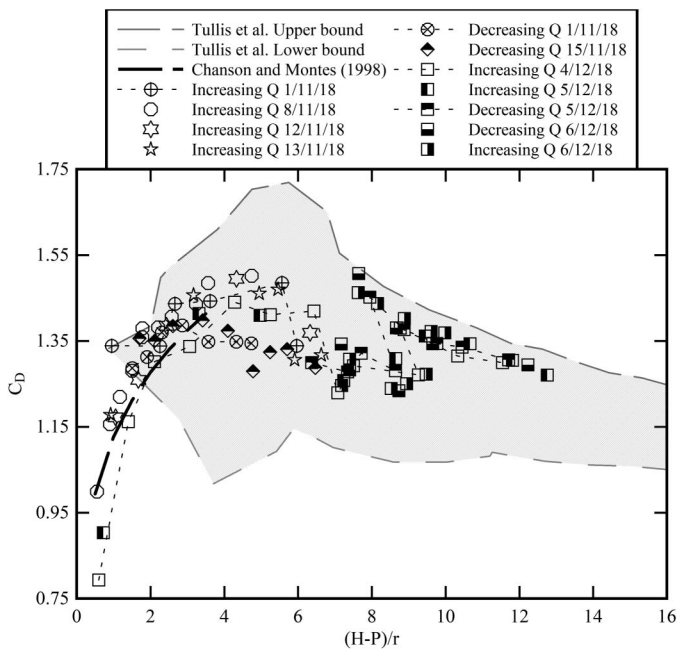
**Fig. 6.** Dimensionless discharge coefficient data over half-round circular crested weirs ($r = 0.010$ m, $P = 0.25$ m)—comparison between all data sets reported by Tullis et al. (2019) including current study (black symbols)

and nappe detachment. The periods of the cyclic pattern were typically between 10 and 12 min, although some unusually wider range of periods, from 1 to 12 min, was observed for $(d - P)/P = 0.34$ (Fig. 4). For that discharge, large transverse fluctuations of the lower nappe impingement perimeter were seen (Fig. 4). Movies S1, S2, and S3 (Supplementary Data and Table S1) present video recordings of the transverse nappe instabilities along the lower nappe impingement with the receiving pool of water. The high-speed recordings (Movies S2 and S3) provide fine details of the wavy nature of the nappe impingement perimeter. Fig. 4 presents a photograph of the lower nappe impacting on the pool of water.

## Basic Flow Characteristics

In a rectangular horizontal channel with hydrostatic pressure distribution, the flow depth at critical flow conditions is $d_c = (q^2/g)^{1/3}$. At the crest of a half-round circular crested weir, the streamline curvature implies a pressure gradient less than hydrostatic (Fawer 1937; Ramamurthy and Vo 1993). The flow depth at the crest of circular weirs is thus expected to differ from $d_c$. Careful measurements of the depth at the crest were undertaken, and the data are presented on Fig. 5(a). Fig. 5(a) compares the current data set to previous observations (Fawer 1937; Vo 1992; Chanson and Montes 1998). With the current data, the water depth at the weir crest was less than the critical flow depth as previously documented (Chanson and Montes 1998; Castro-Orgaz et al. 2008), and the mean value was $d_{crest}/d_c = 0.74$, irrespective of the experimental procedure (increasing/decreasing discharges). Although the present finding suggested a lower $d_{crest}/d_c$ ratio than past data (Fawer 1937; Vo 1992; Chanson and Montes 1998), it covered a much broader range of flow conditions.

Experimental observations of dimensionless discharge coefficients are reported in Fig. 5(b). Fig. 5(b) presents the discharge coefficient as a function of the dimensionless head above crest

$(H - P)/r$ (Fig. 1). In Fig. 5, the legends state whether the data sets were collected with increasing or decreasing discharges. Thin dotted lines connect experimental observations to emphasize the experimental procedure (Fig. 5). The head-discharge data indicated a monotonic increase in the discharge coefficient with an increasing dimensionless head above the crest for $(H - P)/r < 4$–5 [Fig. 5(b)]. The discharge coefficient was larger than unity for $(H - P)/r > 1$, i.e., the discharge on the rounded weir was larger than that on a broad crest [Fig. 5(b), dashed line] for a given upstream head. The present data set is further compared to previous observations [Fig. 5(b)] (Fawer 1937; Vo 1992; Sarginson 1972; Chanson and Montes 1998). The agreement was generally reasonable for $(H - P)/r < 3.5$. However, the present data showed a broad scatter for $4 < (H - P)/r < 11$, which was caused by some nonlinearity and hysteresis of the hydrodynamic system. Within that range, i.e., $4 < (H - P)/r < 11$, several experiments presented two different data points for the same water discharge, i.e., one for the attached nappe and another for the detached nappe.

The present data were further compared to 19 different data sets, collected in hydraulic laboratories across Asia, Europe, North America, and South America with the same weir height $P$ and radius $r$ (Tullis et al. 2019). Note that the current data set was compiled as one of the 20 data sets reported by Tullis et al. (2019). For $2 < (H - P)/r < 11$, the present data scatter was consistent with the cloud of data points presented by Tullis et al. (2019) (Fig. 6). While not a definitive explanation, the comparison hinted that (1) the hydrodynamic instabilities and hysteresis of circular weir overflow might be responsible to a large extent for the scatter and variability of results on half-round circular-crested weirs (Fig. 6); and (2) the experimental procedure must be developed to include long-duration observations, allowing a visualization of the nappe instabilities.

## Conclusion

The current physical study was undertaken with an unventilated half-round circular weir that had a relatively small radius of curvature. On the basis of a detailed investigation under controlled flow conditions, the observations demonstrated that half-round circular weir overflow may be a very complicated flow motion. The data showed some hysteresis, with different results depending on whether the experiments were conducted with increasing or decreasing discharges at $0.08 < (d - P)/P < 0.35$. Large hydrodynamic instabilities were linked to the absence of nappe ventilation. Long-duration cyclic behaviors were recorded for $0.285 < (d - P)/P < 0.35$, including large transverse instabilities of the lower nappe impingement into the body of water. It is important to note that the same parameters $P$ and $r$ were used in the present study and the data sets reported by Tullis et al. (2019). In turn, the generalization of conclusions and the extrapolation of results to other dimensions might need to be tested further.

The present results showed further the importance of the quality of experimental setup and expertise of the individual experimentalist. In the future, it would be recommended to conduct such experimental investigations, in such a way that the flow would be allowed to settle for 30 min before any reading, and to observe for at least 12–15 min the occurrence of any cyclic behavior. Further investigations might include detailed nonintrusive velocity measurements at the crest, as performed by Vo (1992), and in the falling nappe, instantaneous weir invert pressure, and nappe cavity pressure fluctuation recordings, as well as performing the same study in larger physical and numerical computational fluid dynamics models.

© ASCE                                    04020008-5                                    J. Irrig. Drain. Eng.

J. Irrig. Drain Eng., 2020, 146(6): 04020008

## Data Availability Statement

Some or all data, models, or code that support the findings of this study are available from the corresponding author upon reasonable request. These include the tabular data corresponding to the data presented in Figs. 5(b).

## Acknowledgments

## Notation

*The following symbols are used in this paper:*

$B$ = channel width (m);
$C_D$ = dimensionless discharge coefficient;
$d$ = upstream water depth (m);
$d_c$ = critical flow depth (m);
$d_{crest}$ = water depth (m) at weir crest;
$g$ = gravity acceleration (m/s$^2$): $g = 9.794$ m/s$^2$ in Brisbane, Australia;
$H$ = upstream total head (m);
$h$ = water depth along weir wall (m);
$P$ = weir height (m);
$P_{atm}$ = atmospheric pressure (m);
$P_v$ = vapor pressure (Pa);
$P_{wall}$ = invert pressure (Pa);
$Q$ = water discharge (m$^3$/s);
$q$ = water discharge per unit width (m$^2$/s): $q = Q/B$;
$r$ = circular radius (m) of weir crest;
$S_0$ = bed slope: $S_0 = \sin \theta$;
$V$ = velocity (m/s);
$\beta$ = momentum correction coefficient;
$\delta$ = dimensionless term such that $\cos \delta = 1 - 2 \times \beta_{crest} \times C_D^2 \times \Lambda_{crest}^2$;
$\phi$ = radial coordinate;
$\Lambda$ = pressure correction coefficient;
$\theta$ = angle between bed slope and horizontal; and
$\sigma_c$ = critical cavitation number at which cavitation starts to appear.

### Subscript

$c$ = critical flow conditions; and
crest = weir crest flow conditions.

## Supplemental Data

Table S1 and Movies S1–S3 are available only in the ASCE Library (www.ascelibrary.org). Movie S1 shows some transverse nappe instabilities in real time. Movies S2 and S3 present some high-speed movies (240 fps) of large transverse nappe instabilities. The high-speed recordings provide fine temporal details of the wavy nature of the nappe impingement perimeter. Table S1 lists the details of the experimental flow conditions for each movie.

## References

Bakhmeteff, B. A. 1912. *O neravnomernom dwijenii jidkosti v otkrytom rusle (Varied flow in open channel).* [In Russian.] St. Petersburg, Russia: Worldwide Assurance for Employees of Public Agencies.

Bakhmeteff, B. A. 1932. *Hydraulics of open channels*. 1st ed. New York: McGraw-Hill.

Bos, M. G. 1976. *Discharge measurement structures*. Publication No. 161 (also Publication No. 20, ILRI, Wageningen, Netherlands). Delft, Netherlands: Delft Hydraulic Laboratory.

Castro-Orgaz, O., J. V. Giraldez, and J. L. Ayuso. 2008. "Critical flow over circular crested weirs." *J. Hydraul. Eng.* 134 (11): 1661–1664. https://doi.org/10.1061/(ASCE)0733-9429(2008)134:11(1661).

Chanson, H. 1995. *Hydraulic design of stepped cascades, channels, weirs and spillways*. Oxford, UK: Pergamon.

Chanson, H. 1997. "A review of the overflow of inflatable flexible membrane dams." *Aust. Civ. Struct. Eng. Trans.* CE41 (2–3): 107–116.

Chanson, H. 1998. "Hydraulics of rubber dam overflow: A simple design approach." In Vol. 1 of *Proc., 13th Australasian Fluid Mech. Conf.*, edited by M. C. Thompson and K. Hourigan, 255–258. Perth Western, Australia: Australasian Fluid Mechanics Society.

Chanson, H. 2004. *The hydraulics of open channel flow: An introduction*. 2nd ed. Oxford, UK: Butterworth-Heinemann.

Chanson, H. 2006. "Minimum specific energy and critical flow conditions in open channels." *J. Irrig. Drain. Eng.* 132 (5): 498–502. https://doi.org/10.1061/(ASCE)0733-9437(2006)132:5(498).

Chanson, H. 2008. "Minimum specific energy and critical flow conditions in open channels—Closure." *J. Irrig. Drain. Eng.* 134 (6): 883–887. https://doi.org/10.1061/(ASCE)0733-9437(2008)134:6(883).

Chanson, H., and J. S. Montes. 1998. "Overflow characteristics of circular weirs: Effect of inflow conditions." *J. Irrig. Drain. Eng.* 124 (3): 152–162. https://doi.org/10.1061/(ASCE)0733-9437(1998)124:3(152).

Chanson, H., and H. Wang. 2013. "Unsteady discharge calibration of a large V-notch weir." *Flow Meas. Instrum.* 29 (Mar): 19–24. https://doi.org/10.1016/j.flowmeasinst.2012.10.010.

Fawer, C. 1937. "Etude de quelques ecoulements permanents à filets courbes (Study of some steady flows with curved streamlines)." [In French.] Ph.D. thesis, Engineering School, Imprimerie La Concorde.

Fekete, G. I. 1963. *Coanda flow of a two-dimensional wall jet on the outside of a circular cylinder.* Rep. No. 63-11. Montréal: Dept. of Mechanical Engineering, McGill Univ.

Henderson, F. M. 1966. *Open channel flow*. New York: MacMillan.

Knapp, R. T., J. W. Daily, and F. G. Hammitt. 1970. *Cavitation*. New York: McGraw-Hill.

Miller, D. S. 1994. *Discharge characteristics. IAHR hydraulic structures design manual No. 8, hydraulic design considerations*. Rotterdam, Netherlands: A.A. Balkema.

Montes, J. S. 1998. *Hydraulics of open channel flow*. New York: ASCE Press.

Moore, W. L. 1943. "Energy loss at the base of a free overfall." *Transactions* 108 (Nov): 1343–1360.

Novak, P., A. I. B. Moffat, C. Nalluri, and R. Narayanan. 2001. *Hydraulic structures*. 3rd ed. London: Spon Press.

Ogihara, K., and T. Maramatsu. 1985. "Rubber dam: Causes of oscillation of rubber dams and countermeasures." In *Proc., 21st IAHR Biennial Congress*, 600–604. Beijing: International Association for Hydraulic Research.

Ramamurthy, A. S., and N. D. Vo. 1993. "Application of Dressler theory to weir flow." *J. Appl. Mech. Trans.* 60 (1): 163–166. https://doi.org/10.1115/1.2900740.

Robertson, J. M. 1965. *Hydrodynamics in theory and application*. London: Prentice-Hall International.

Sarginson, E. J. 1972. "The influence of surface tension on weir flow." *J. Hydraul. Res.* 10 (4): 431–446. https://doi.org/10.1080/00221687209500034.

Sarpkaya, T. 1968. *The deflection of plane turbulent jets by convex walls*. US Government Research Rep. No. AD 673249. Monterey, CA: Naval Postgraduate School.

Tullis, B. P., B. M. Crookston, and D. B. Bung. 2019. "Weir head-discharge relationships: A multilab exercise." In *Proc., 38th IAHR World*

© ASCE      04020008-6      J. Irrig. Drain. Eng.

J. Irrig. Drain. Eng., 2020, 146(6): 04020008

*Congress, Panama*. Beijing: International Association for Hydraulic Research. https://doi.org/10.3850/38WC092019-0806.

USBR (United States Bureau of Reclamation). 1987. *Design of small dams*. 3rd ed. Denver: Bureau of Reclamation, US Dept. of the Interior.

Vo, N. D. 1992. "Characteristics of curvilinear flow past circular-crested weirs." Ph.D. thesis, Dept. of Civil Engineering, Concordia Univ.

Wu, P. H., and R. H. Plaut. 1996. "Analysis of the vibrations of inflatable dams under overflow conditions." *Thin Walled Struct.* 26 (4): 241–259. https://doi.org/10.1016/0263-8231(96)00030-4.

# Half-Round Circular Crested Weir: On Hysteresis, Instabilities, and Head–Discharge Relationship

Hubert Chanson

Table S1 - Movies of nappe instabilities above a half-round circular crest weir

| Movie | Filename | Camera | Movie details | Flow conditions | Comments |
|-------|----------|--------|---------------|-----------------|----------|
| S1 | IMGP1089.mov | Pentax K-3 | HD (1920×1080 pixels), 50 fps | $Q = 0.0193$ m$^3$/s, d = 0.326 m, $d_{crest} = 0.058$ m, H = 0.3271 m, $C_D = 1.32$, increasing discharge experiment | Detached nappe overflow with large transverse nappe instabilities |
| S2 | CIMG5836.mov | Casio EX-10 | 512×384 pixels, 240 fps | $Q = 0.0217$ m$^3$/s, d = 0.336 m, $d_{crest} = 0.0675$ m, H = 0.3373 m, $C_D = 1.23$, increasing discharge experiment | High-speed movie of detached nappe overflow with small air cavity and large transverse nappe instabilities |
| S3 | CIMG5862.mov | Casio EX-10 | 512×384 pixels, 240 fps | $Q = 0.0253$ m$^3$/s, d = 0.3395 m, H = 0.3413 m, $C_D = 1.35$, steady discharge experiment | High-speed movie of detached nappe overflow with very large transverse nappe instabilities |